Applied Physics B (2021) 127:77
https://doi.org/10.1007/s00340-021-07627-4

Applied Physics B
Lasers and Optics

RAPID COMMUNICATION

High-efficiency CW and passively Q-switched operation of a 2050 nm L-shaped Tm^{3+}:Y_2O_3 ceramic laser in-band fiber-laser pumped at 1670 nm

O. L. Antipov[1,2] · Yu. A. Getmanovskiy[1,3] · A. A. Dobrynin[2] · H. T. Huang[4] · D. Y. Shen[4] · J. Wang[4] · S. S. Balabanov[5]

Received: 9 January 2021 / Accepted: 20 April 2021 / Published online: 29 April 2021

Abstract
A Tm^{3+}:Y_2O_3 ceramic laser with the L-shaped cavity in-band pumped by a fiber laser at 1670 nm was studied in the CW and passively Q-switched regimes. The CW laser was tunable in the range between 2046 and 2054 nm. The output power reached up to 4.9 W and the average slope efficiency was 75% in the high-quality single-transverse-mode beam The highest CW output power in the multi-transverse-mode beam was 12 W. A Cr^{2+}:ZnSe saturable absorber was used to achieve the Q-switched operation at 2051 nm with the average power of up to 1.3 W in the single transverse mode, at the pulse repetition rate of 2–10 kHz and the pulse width of 80–150 ns.

1 Introduction

Solid-state lasers at 2 μm have a variety of applications in surgery, materials processing, environmental monitoring, gas detection and pumping of mid-IR optical parametric oscillators [1, 2]. Furthermore, multi-wavelength 2 μm lasers can be used for the difference frequency generation in the far-IR and terahertz spectral regions [3, 4].

Lasers based on Tm^{3+}-doped sesquioxide ceramics such as Lu_2O_3, Y_2O_3 and $(Lu,Sc)_2O_3$ have demonstrated high average power and high efficiency in the 2 μm output [4–7]. The CW, actively and passively Q-switched, and mode locking regimes were previously achieved at 2 μm in Tm^{3+}-doped sesquioxide ceramic lasers [4–12]. In particular, the Tm^{3+}:Y_2O_3 ceramic lasers diode-pumped at 780–810 nm were demonstrated in the CW and Q-switched modes [6, 11, 12].

The in-band pumping of the $^3H_6$-$^3F_4$ Tm^{3+}-ion transition enables the high-efficiency and high-power operation of Tm^{3+}-doped lasers at 1900–2100 nm with a low quantum defect [13–19]. Direct excitation of Tm^{3+} ions into the upper laser level $^3F_4$ results in the reduced thermal load and high laser efficiency compared to the diode pumping by $^3H_4$ level with the subsequent cross relaxation $(^3H_4,^3H_6) \rightarrow (^3F_4,^3F_4)$ of the Tm^{3+} ions with phonon assistance (Fig. 1a). The Tm^{3+}:YAG and Tm^{3+}:Lu_2O_3 ceramic lasers and amplifiers with the in-band pumping at 1615 nm and 1670–1678 nm were recently reported in a number of papers [15, 16, 18].

✉ O. L. Antipov
oleg_antipov@yahoo.com

Yu. A. Getmanovskiy
getmanovskij@yandex.ru

A. A. Dobrynin
player676@yandex.ru

H. T. Huang
hht840211@163.com

D. Y. Shen
shendy@fudan.edu.cn

J. Wang
jwang025@e.ntu.edu.sg

S. S. Balabanov
balabanov@ihps-nnov.ru

[1] Institute of Applied Physics of the Russian Academy of Sciences (IAP RAS), 46 Ulyanov St., Nizhny Novgorod 603950, Russia

[2] Nizhny Novgorod State University, 23 Gagarin Av., Nizhny Novgorod 603950, Russia

[3] Nizhny Novgorod State Technical University, 24 Minin St., Nizhny Novgorod 603950, Russia

[4] School of Physics and Electronic Engineering, Jiangsu Key Laboratory of Advanced Laser Materials and Devices, Jiangsu Normal University, Xuzhou 221116, China

[5] Institute of Chemistry of High-Purity Substances of the Russian Academy of Sciences (IChHPS RAS), 49 Tropinin St., Nizhny Novgorod 603951, Russia

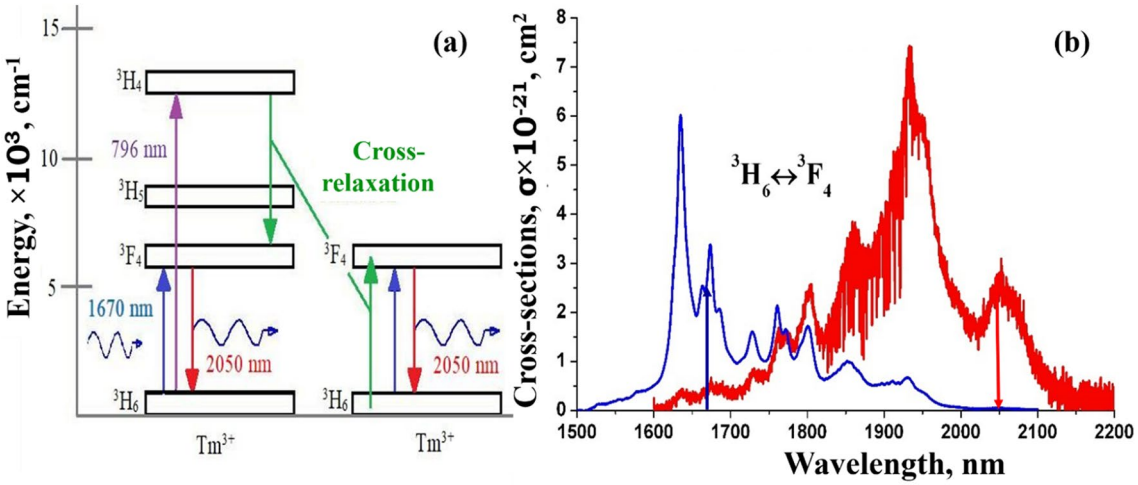

Fig. 1 The energy level diagram of Tm^{3+} ions in a Tm^{3+}:Y_2O_3 material with the absorption and emission transitions in different colors (**a**) [20]; the absorption (blue) and emission (red) cross-sections of Tm^{3+}:Y_2O_3 ceramics for the transition term of $^3H_6$-$^3F_4$ [6] (**b**). The vertical arrows indicate the pumping wavelength of 1670 nm (blue) or 796 nm (violet), the laser operation wavelength of 2050 nm (red), and the cross-relaxation process (green)

In this paper we report, for the first time to the best of our knowledge, a Tm^{3+}:Y_2O_3 ceramic laser in-band pumped by a fiber laser at 1670 nm. The Tm^{3+}:Y_2O_3 ceramic laser with an L-shaped cavity operated either in the CW regime at 2046–2051 nm, or in a Q-switched regime at kHz repetition rate when a Cr^{2+}:ZnSe saturable absorber was inserted into the laser cavity. New pump configuration enabled higher efficiency compared to the diode-pumped Tm^{3+}:Y_2O_3 ceramic lasers.

2 Experimental setup

A Y_2O_3 ceramic rod with the 6.0 mm diameter and 16 mm length was doped with 1 at. % of Tm^{3+} ions (Jiangsu Normal University). Both end surfaces of the rod were AR-coated at 1.67 µm and 2 µm. The ceramic rod was wrapped in indium foil and inserted into a copper radiator with the temperature stabilized between 8 and 10 ºC.

The high optical quality of the rear-earth doped Y_2O_3 ceramics was recently reported [21]. It was reviled in our tests by probing the Tm^{3+}:Y_2O_3 ceramic element with a laser beam. A far-field scattering background produced by a single-mode He–Ne laser at 633 nm after its propagation through the sample was found to be comparable to the scattering background measured in the Tm^{3+}:Lu_2O_3 ceramics produced by "Konoshima Chemicals, Co" (Fig. 2a–c) [5]. In addition to that, the Tm^{3+}:Y_2O_3 ceramics was probed with a fiber laser at 1567 nm that showed a high quality beam profile in the far-field: the beam-quality parameter M^2 (determined using the knife-edge method, ISO standard 11,146–1 [22]) was ≤ 1.1 for the initial probing beam and became ≤ 1.3 after passing through the Tm^{3+}:Y_2O_3 ceramic rod (Fig. 2d, e).

The Tm^{3+}:Y_2O_3 ceramic rod was pumped at 1670 nm by a CW Raman-shifted erbium fiber laser (IPG Photonics). The maximum output power in a single transverse mode at 1670 nm reached 52.5 W. The Gaussian pump beam with the beam quality $M^2 \approx 1.1$ was focused by a two-lens telescope (LT) to a beam radius of $w_p \approx 220$ µm, measured at e^{-2} intensity, into the ceramic element.

The absorption spectrum of the Tm^{3+}:Y_2O_3 ceramics indicates a local maximum near 1680 nm with the cross-section of $\sigma_{ab} \approx 2.4 \times 10^{-21}$ cm^2 [6] (Fig. 1b). The absorption coefficient ($\alpha_{ab} = \sigma_{ab} N$) at 1670 nm can be estimated at 0.48 cm^{-1} assuming the $N \approx 2 \times 10^{20}$ cm^{-3} concentration of Tm^{3+} ions in the active C_2-symmetry sites [2]. The measured small-signal absorption in the Tm^{3+}:Y_2O_3 ceramic rod confirmed this estimation: the single-pass absorption was ~ 48–50% of the incident power.

The ceramic laser had an L-shaped cavity formed by three mirrors (Fig. 3): a dichroic 45-degree pump plane mirror M_2 with the 99.4–99.8% reflectivity at 1.9–2.1 µm and 98% transmittance at 1.67 µm; a plane rear mirror M_1 with the high reflectivity (≥ 99.7%) both at 1.67 and 2 µm; a curved output coupler M_3 with the radius of curvature of 200 mm and the transmittance of ~ 17% at 2050 nm and ~ 51% at 1940 nm. The chosen cavity layout provided a double pass of the pump beam through the ceramic rod and minimized the influence of the pump on a Cr^{2+}:ZnSe saturable absorber positioned in the output leg.

The length of both cavity arms was varied to achieve the highest output power and the best lasing beam quality. The distance between the rod surface and the mirror M_1 was

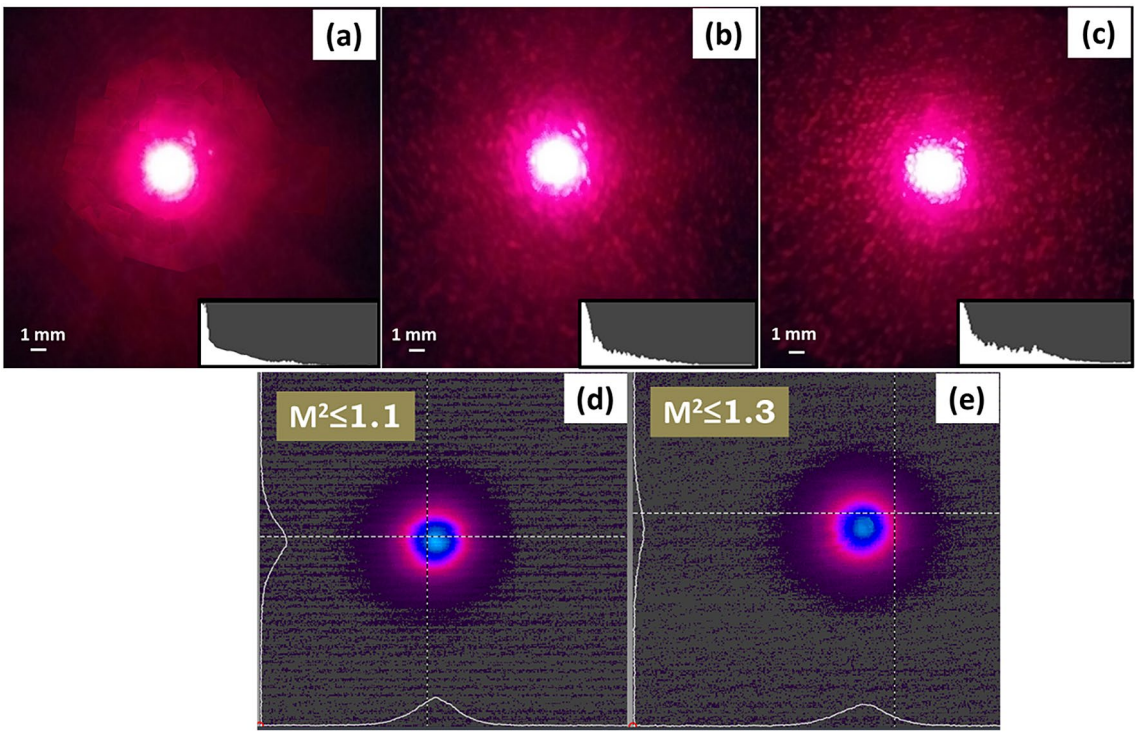

Fig. 2 Far-field images (photos) of the probing laser beam at 633 nm without any ceramics (**a**), and transmitted through the $Tm^{3+}:Y_2O_3$ ceramic rod with the length of 16 mm (**b**), or through the $Tm^{3+}:Lu_2O_3$ ceramic rod with the same length (**c**). The inserts show the luminosity histograms. The far-field images of a probing single-mode fiber-laser beam at 1567 nm (registered by PYROCAM IV) without any ceramics and transmitted through the $Tm^{3+}:Y_2O_3$ ceramic rod are shown in **d** and **e**, respectively

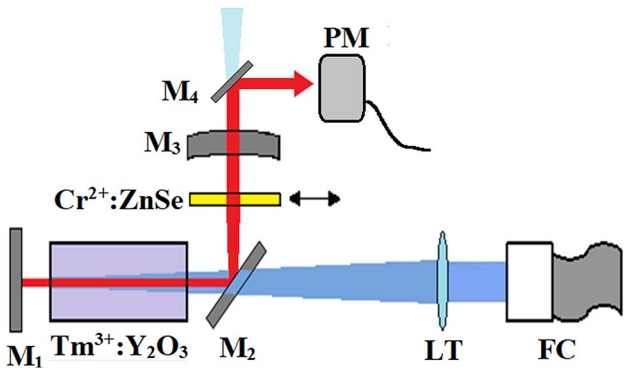

Fig. 3 Schematic of the $Tm^{3+}:Y_2O_3$ ceramics laser with (or without) a Cr^{2+}:ZnSe saturable absorber

varied between 3 and 20 mm, the distance between the input rod surface and the pump mirror M_2 was 5–30 mm, and the output arm between mirrors M_2 and M_3 was 55–100 mm in length. The total physical cavity length (L) was varied from 106 to 130 mm. The cavity configuration was close to semi-confocal. The laser output was filtered from the residual pump by a dichroic mirror M_4 and measured by a power meter (Ophir "30(150)A-BB-18ROHS" power sensor with "StarBright" power meter (PM)).

The passive Q-switched operation was achieved by inserting a Cr^{2+}:ZnSe element into the output leg of the cavity (see description in paragraph 4).

3 CW operation

The absorbed pump threshold for the CW operation was ~ 4.3 W. The pump absorption after a double pass through the rod was estimated at 70% of the incident power. The Gaussian beam output of 4.9 W was measured at the absorbed pump power of 10.5 W (Fig. 4). The optical-to-optical efficiency of the laser reached 46% with respect to the absorbed pump power.

The Ophir-Spiricon "PYROCAM IV" beam profiler was used to analyze the laser output. The divergence angle and beam quality were analyzed in the focal zone of a lens with the 70 cm focal length using the knife-edge method (ISO standard 11146-1) [22]. The beam quality was $M^2 \leq 1.5$ at the output power of 4.9 W in a single-transverse-mode regime. The multi-transverse-mode operation of the ceramic laser with the higher output power was observed when the absorbed pump exceeded 10.5 W. The highest output power of 12 W was registered in the multi-transverse-mode laser beam at the absorbed pump power of 33 W.

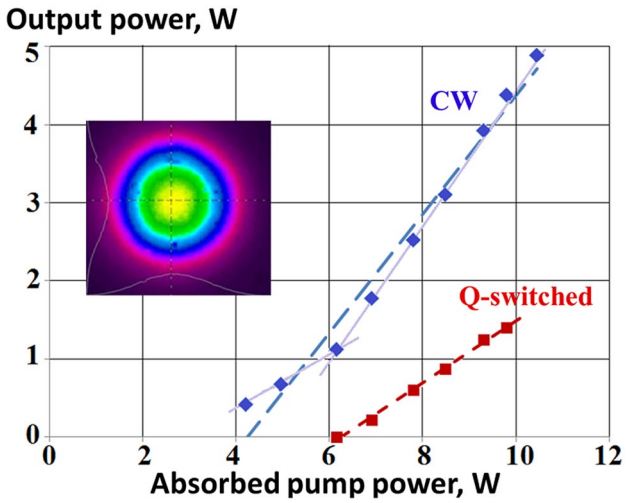

Fig. 4 Output power of the Tm^{3+}:Y_2O_3 ceramic laser in the CW and passively Q-switched regimes vs absorbed pump power. The insert shows the PYROCAM image of the output beam, the dashed lines are the average trends, the violet solid lines are the differential lines

The slope efficiency of a single-transverse-mode CW operation, defined as the derivative of the output power with respect to the absorbed pump, has a nonlinear behavior: the differential efficiency reached ~ 37% at the low absorbed pump power (from 3 to 6 W), however at the higher absorbed pump (from 6 to 10.5 W) the differential efficiency increased to ~ 83% (see the violet solid lines in Fig. 4). A double increase of the differential efficiency at the higher pump in a quasi-three-level Tm^{3+}:Y_2O_3 ceramic laser can be explained by the improved mode matching between the pump and lasing beams in a cavity with a stronger thermal lens [23]. The average slope efficiency determined by the trend line of a single-transverse-mode operation was estimated to be ~ 75% (see the blue dashed line in Fig. 4). This value is significantly higher than the 40% slope efficiency of a diode-pumped laser based on the same ceramics diode-pumped at 785 nm [11], and higher than the 59% slope efficiency of Tm-doped sesquioxide (Lu_2O_3 and Sc_2O_3) lasers under the 796 nm diode pumping [1, 2]. The slope efficiency of the manufactured Tm^{3+}:Y_2O_3 laser is comparable to the efficiency achieved in other Tm^{3+}:Lu_2O_3 ceramic lasers under in-band pumping at 1670 nm [18], and in the laser based on Tm^{3+}:Sc_2O_3 single crystal under 1611 nm pumping [17].

The output spectrum was analyzed by a monochromator M150 (SOLAR Laser Systems, Belarus), HAMAMATSU InGaAs PIN G8422-03 photodiode combined with in-house made software. It was found to depend on both the pump power and configuration of the cavity (Fig. 3). Specifically, close to the lasing threshold the output spectrum consisted of two peaks centered within the 2049–2051 nm range (Fig. 5a). Multiple peaks within the 2046–2053 nm range were registered when the laser was operated far above the threshold (Fig. 5b). The number of peaks and their corresponding central frequencies were unstable during the laser operation.

The complicated relaxation oscillations of the output power with a specific period on a microsecond time scale were registered in the CW regime. Similar multi-wavelength operation has been previously observed in diode-pumped Tm^{3+}:Y_2O_3 ceramic lasers [6, 11]. The unstable output wavelength indicates the mode competition inside the ceramic laser. However, in the fiber-pumped ceramic laser, the operation wavelength remained within the 2046–2054 nm range without jumping to a shorter band at 1930–1950 nm at higher pump intensity. This can be attributed to the reflectivity spectra of the mirrors which discriminated the shorter wavelength operation of the ceramic laser.

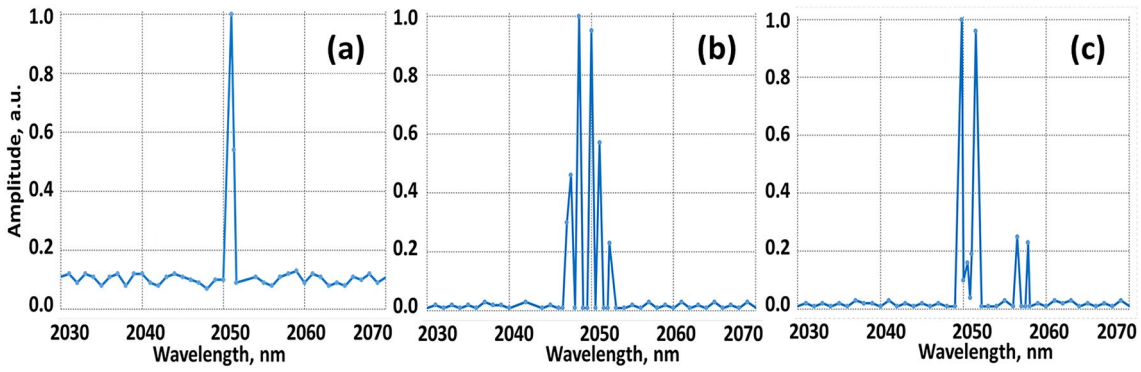

Fig. 5 Operation spectra of the Tm^{3+}:Y_2O_3 ceramic laser in the CW (**a**, **b**) and passively Q-switched (**c**) regimes at different levels of the absorbed pump power: near-threshold at 4.5 W (**a**), far above the threshold at 8.5 W (**b**) and in a Q-switched mode at 9.4 W (**c**)

4 Passively Q-switch operation

Two Cr^{2+}:ZnSe elements with the diameter of 12.7 mm and thickness of 2 or 3 mm (IChHPS RAS) were used to achieve passive Q-switching. The working surfaces of the Cr^{2+}:ZnSe elements were AR-coated at 2 µm. The Cr^{2+}:ZnSe plates were inserted into a copper holder with no additional temperature stabilization. The initial (small-signal) transmission of a 2-m-thick Cr^{2+}:ZnSe element was measured to be ~ 90% at 1940 nm and ~ 93% at 2050 nm; the second Cr^{2+}:ZnSe element with the thickness of 3 mm had the initial transmission of ~ 80% at 1940 nm and ~ 84% at 2066 nm. The Cr^{2+}:ZnSe saturable absorber was placed into the output leg of the cavity 20–30 mm away from the output coupler M_3 (Fig. 3). The position of the element inside the cavity was varied to achieve the highest average power.

The 2-mm Cr^{2+}:ZnSe saturable absorber resulted in the higher average output power compared to the 3-mm Cr^{2+}:ZnSe element. The Q-switched laser with the 2-mm Cr^{2+}:ZnSe element operated with high beam quality and the average power of up to 1.3 W (Fig. 4). The slope efficiency of a passively Q-switched in-band pumped Tm^{3+}:Y_2O_3 ceramic laser was determined to be 40% (see the dashed red trend line in Fig. 4). It was much higher than that of a diode-pumped laser based on the same ceramics both in the actively and passively Q-switched regimes [11, 12]. However, the slope efficiency of the in-band pumped Tm^{3+}:Y_2O_3 ceramic laser in a Q-switched regime was found to be significantly lower than the slope efficiency of the same laser in a CW regime. This could be attributed firstly, to the optical losses inside the polycrystalline Cr^{2+}:ZnSe saturable absorber, and secondly, to the increase of up-conversion in Tm^{3+}:Y_2O_3 ceramics due to higher population of the upper laser $^3F_4$ level.

The pulse repetition rate (PRR) increased while the pulse width (PW) decreased with increase in the absorbed pump power: at 6.3 W of the pump PRR and PW were 1.6–1.8 kHz and 140–150 ns, respectively (Fig. 6a, b); once the pump

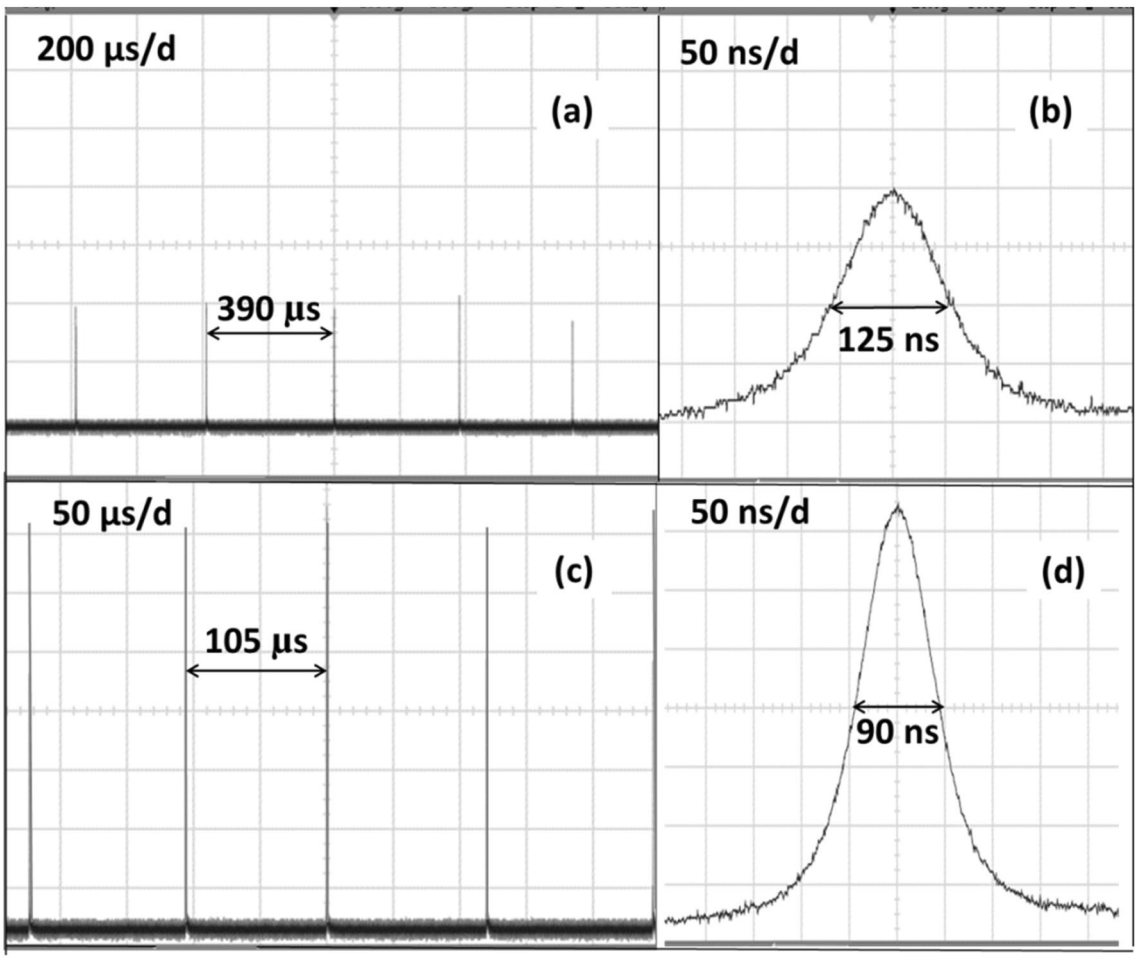

Fig. 6 The Q-switched Tm^{3+}:Y_2O_3 laser operation: the pulse trains (**a**, **c**) and the single pulses inside the train (**b**, **d**) at the absorbed pump power of 6.8 W (**a**, **b**) and 9.4 W (**c**, **d**)

reached 9.4 W, PRR increased to 8–9 kHz and PW decreased to 80–90 ns (Fig. 6c, d). Figure 7 indicates the PRR and PW dependences vs the absorbed pump power from 6.5 to 9.4 W. The peak power of the Q-switch pulses reached 1.7–1.8 kW at 6–9 kHz of PRR. The pulse-to-pulse instability of the peak power, PRR and PW was less than 10% when the absorbed pump power was under 9 W and grew sharply to 2–3 × the initial value when the absorbed pump reached over 9.4 W.

The output spectrum of the Q-switched laser contained a few peaks within the wavelength range of 2046–2058 nm. The number of peaks and their central frequencies were unstable during laser operation with a time scale in the range of seconds.

5 Discussion

There are several reasons for the higher efficiency of in-band pumped Tm-doped lasers compared to lasers with the 800-nm diode pumping. The 800-nm diode pumping of the $^3H_6 \rightarrow {}^3H_4$ transition promotes Tm^{3+} ions to a high-energy $^3H_4$ level followed by the phonon-assisted cross-relaxation of a Tm^{3+} ion pair $(^3H_4,{}^3H_6) \rightarrow ({}^3F_4,{}^3F_4)$ with populating the high $^3F_4$ level of the 2-μm laser transition. Even assuming that the cross-relaxation promotes two ions to the $^3F_4$ level for each absorbed pump photon, the quantum efficiency of the 1670-nm pump is higher than the quantum efficiency of the "2-for-1" diode pump at 800 nm. Moreover, there are other effects competing with the cross-relaxation that cause depopulation of the pumped $^3H_4$ level in the Tm-doped laser materials. These effects include the nonradiative relaxation though a $^3H_5$ level, radiative near-IR $^3H_4 \rightarrow {}^3H_6$ transitions, up-conversion and the exited state absorption of the 800 nm radiation [24–26]. These processes decrease the efficiency of diode pumped thulium lasers due to decrease of the cross-relaxation rate and increase of the thermal load. In addition to that, the Tm^{3+} ions concentration in a diode-pumped laser medium is typically set to 2–4 at. % to assist the cross-relaxation process. Even though this does lead to higher efficiency in diode-pumped thulium lasers, the increased ion concentration at fixed spatial dimensions of the active medium increases up-conversion from the higher $^3F_4$ level of the laser transition (that is followed by the short-wavelength luminescence) and reabsorption from the $^3H_6$ state due to the quasi-three-level nature of a thulium-doped medium with faster nonradiative decay resulting from energy migration between Tm^{3+} ions [14, 15, 24, 27].

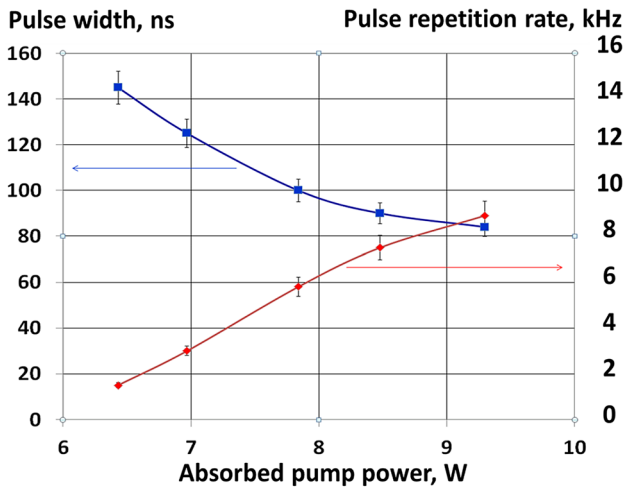

Fig. 7 The pulse width (blue) and the pulse repetition rate (red) vs the absorbed pump power

Compared to that, the in-band pumping does not require a high concentration of Tm^{3+} ions. In our tests on the $Tm^{3+}:Y_2O_3$ ceramic laser, we used the dopant concentration as low as 1 at. %, which was shown to be substantial for the high-efficiency laser operation. Since the Tm^{3+} ion concentration was reduced, the visible up-conversion luminescence from $Tm^{3+}:Y_2O_3$ ceramics under the in-band pumping was significantly weaker compared to the highly doped samples under diode-pumped conditions.

Another benefit of the in-band fiber-laser pumping is the high beam quality of the lasing. In our experiments with $Tm^{3+}:Y_2O_3$ ceramics, the pump beam from the fiber laser at 1670 nm was focused into the active rod to provide the best overlap between the pump and lasing beams, which undoubtedly increased the overall laser efficiency.

No sign of the optical damage of $Tm^{3+}:Y_2O_3$ ceramics was observed at the pump beam intensity of up to ~ 60 kW/cm^2 in the CW regime and at the laser fluence of up to ~ 1 J/cm^2 in the Q-switched regime. However, the power scaling of the single-transverse-mode beam was limited by the rather strong thermal lens effect in the ceramics.

6 Conclusion

In summary, the $Tm^{3+}:Y_2O_3$ ceramic laser with the in-band fiber-laser pumping and the L-shaped cavity demonstrated high efficiency both in the CW and passively Q-switched regimes at wavelengths near 2050 nm. The CW output power reached 4.9 W in a high-quality beam with the average slope efficiency of 75% and the optical-to-optical efficiency of 47%. The demonstrated slope efficiency of the single-transverse-mode $Tm^{3+}:Y_2O_3$ ceramic laser with the in-band fiber-laser pumping far exceeded the efficiency of the laser with the diode pumping at 800 nm. The optical-to-optical efficiency of the single-transverse-mode operation with respect to the absorbed pump power can be increased by the appropriate choice of length of the active ceramic element and the cavity configuration.

The Cr^{2+}:ZnSe saturable absorber inside the laser cavity provided a passively Q-switched operation, the PRR and the PW were 2–10 kHz and 85–120 ns, respectively. The repetitively pulsed operation of the passively Q-switched ceramic laser with the average power of up to 1.3 W with the slope efficiency of 40% was achieved.

The high efficiency and compact Tm^{3+}:Y_2O_3 ceramic lasers at 2051 nm in CW and passively Q-switched regimes can be used for surgery and material processing.

Funding This research was supported by the Russian Foundation for Basic Research (Grant № 19-32-50094/19) and the Ministry of Science and Higher Education of the Russian Federation, state assignment for the Institute of Applied Physics RAS (project № 0035-2019-0012).

Availability of data and materials All material in the paper is suitable for the open access.

Declarations

Conflict of interest Authors of the present paper have no conflicts of interest with other scientists in the same research field.

References

1. K. Scholle, S. Lamrini, P. Koopmann, P. Fuhrberg, *Frontiers in Guided Wave Optics and Optoelectronics* (Croatia, InTech, 2010).
2. C.H. Krankel, IEEE J. Sel. Top. Quant. Electron. **21**, 1602013–1602113 (2015)
3. D. Creeden, J.C. McCarthy, P.A. Ketteridge, T. Southward, P.G. Schunemann, J.J. Komiak, W. Dove, E.P. Chicklis, IEEE J. Sel. Top. Quant. Electron. **13**, 732–736 (2007)
4. H. Huang, S. Wang, H. Chen, O.L. Antipov, S.S. Balabanov, D. Shen, Opt. Express **27**, 38593–38601 (2019)
5. O.L. Antipov, A.A. Novikov, N.G. Zakharov, A.P. Zinoviev, Opt. Mater. Express **2**, 183–189 (2012)
6. P.A. Ryabochkina, A.N. Chabushkin, Yu.L. Kopylov, V.V. Balashov, K.V. Lopukhin, Quant. Electron. **46**, 597–600 (2016)
7. W. Jing, P. Loiko, J.M. Serres, Y. Wang, E. Vileishnikova, M. Aguilo, F. Diaz, U. Grebner, H. Huang, V. Petrov, X. Mateos, Opt. Mat. Express **7**, 4192–4202 (2017)
8. Z. Zhou, X. Guan, X. Huang, B. Xu, H. Xu, Zh. Caj, X. Xu, P. Liu, D. Li, J. Zhang, J. Xu, Opt. Lett. **42**, 3781–3784 (2017)
9. O. L. Antipov, Yu. A. Getmanovskiy, S. S. Balabanov, S. V. Larin, V. V. Sharkov, Laser Phys. Lett. **18**, 055001 (2021)
10. A.A. Lagatsky, O.L. Antipov, W. Sibbett, Opt. Express **20**, 19349–19354 (2012)
11. H. Wang, H. Huang, P. Liu, L. Jin, D. Shen, J. Zhang, D. Tang, Opt. Mater. Express **7**(2), 296–303 (2017)
12. H. Huang, H. Wang, D. Shen, Opt. Mater. Express **7**, 3147–3154 (2017)
13. F. Cornacchia, A. Di Lieto, P. Maroni, P. Minguzzi, A. Toncelli, M. Tonelli, E. Sorokin, I. Sorokina, Appl. Phys. B. **73**, 191–194 (2001)
14. Yu.L. Kalachev, V.A. Mihailov, V.V. Podreshetnikov, I.A. Shcherbakov, Opt. Commun. **284**, 3357–3360 (2011)
15. Y. Wang, D. Shen, H. Chen, J. Zhang, X. Qin, D. Tang, X. Yang, T. Zhao, Opt. Lett. **36**, 4485–4487 (2011)
16. S. Larin, O. Antipov, V. Sypin, O. Vershinin, Opt. Lett. **39**, 3216–3218 (2014)
17. M. Tokurakawa, Y. Mashiko, C. Kränkel, in Technical Digest of European Conference on Lasers and Electro-Optics (CLEO-Europe 2015), paper CA_12_1 (2015).
18. O. Antipov, A. Novikov, S. Larin, I. Obronov, Opt. Lett. **41**, 2298–2301 (2016)
19. F. Wu, W. Yao, H. Xia, Q. Liu, M. Ding, Y. Zhao, W. Zhou, X. Xu, D. Shen, Opt. Mater. Express **7**, 1289–1294 (2017)
20. Q. Yi, T. Tsuboi, Sh. Zhou, Y. Nakai, H. Lin, H. Teng, Chines Opt. Lett. **10**, 091602 (2012)
21. K. Ning, J. Wang, J. Ma, Zh. Dong, L.B. Kong, D. Tang, Mater. Today Commun. **24**, 101185 (2020)
22. ISO 11146–1:2005 Lasers and laser-related equipment—Test methods for laser beam widths, divergence angles and beam propagation ratios—Part 1: Stigmatic and simple astigmatic beams.
23. T. Taira, W.M. Tulloch, R.L. Byer, Appl. Optics **36**(9), 1867–1874 (1997)
24. A. Brenier, J. Rubin, R. Moncorge, C. Pedrini, J. de Phys. **50**, 1463–1482 (1989)
25. M. Eichhorn, Appl. Phys. B **93**, 269–316 (2008)
26. B.M. Walsh, Laser Phys. **19**, 855–866 (2009)
27. H. Kalaycioglu, A. Sennaroglu, IEEE J. Sel. Top. Quant. Electron. **11**, 573–667 (2005)